PHYSICS

Control of trion-to-exciton conversion in monolayer WS_2 by orbital angular momentum of light

Rahul Kesarwani[1], Kristan Bryan Simbulan[1], Teng-De Huang[1], Yu-Fan Chiang[1], Nai-Chang Yeh[2]*, Yann-Wen Lan[1]*, Ting-Hua Lu[1]*

Controlling the density of exciton and trion quasiparticles in monolayer two-dimensional (2D) materials at room temperature by nondestructive techniques is highly desired for the development of future optoelectronic devices. Here, the effects of different orbital angular momentum (OAM) lights on monolayer tungsten disulfide at both room temperature and low temperatures are investigated, which reveal simultaneously enhanced exciton intensity and suppressed trion intensity in the photoluminescence spectra with increasing topological charge of the OAM light. In addition, the trion-to-exciton conversion efficiency is found to increase rapidly with the OAM light at low laser power and decrease with increasing power. Moreover, the trion binding energy and the concentration of unbound electrons are estimated, which shed light on how these quantities depend on OAM. A phenomenological model is proposed to account for the experimental data. These findings pave a way toward manipulating the exciton emission in 2D materials with OAM light for optoelectronic applications.

INTRODUCTION

Excitons are one of the most studied quasiparticles in modern quantum materials because of their technological relevance to advanced electronic, optoelectronic, and photonics devices (*1*–*3*). Recently, excitonic-based materials have been used in the development of high-performance photodetectors (*4*), light-emitting diodes (*5*), excitonic lasers (*6*), valleytronic transistors (*7*), and optical interconnectors (*8*). Moreover, strong excitonic effects also contribute to nonlinear optical excitations such as two-photon luminescence and high-order harmonic generation (*9*). The wide range of applications associated with exciton quasiparticle may be attributed to strong light-matter interaction that enhances the photoluminescence (PL) and electroluminescence properties of the material (*10*). It is therefore desirable to devise new techniques to control and enhance radiative excitons in existing materials to improve the excitonic-based device applications.

An exciton is a neutral excitation that consists of an electron-hole pair bound by Coulomb interaction in a semiconductor or an insulator (*11*). Much research efforts have been made to improve the excitonic behavior in composite materials, although more attention is still needed to advance the development of excitonic devices (*12*, *13*). Earlier, excitonic devices have been largely based on gallium arsenide (GaAs) quantum dots or quantum wells because of their rich excitonic properties. However, the weak exciton binding energy (<7 meV) in these systems requires operation at low temperatures (near 4 K) (*14*, *15*) and implies ultrashort radiative lifetimes, which are orders of magnitude shorter than that of conventional semiconducting light emitters (*16*). This drawback can be overcome by replacing the host material for excitons with monolayers of transition metal dichalcogenides (TMDs) such as WS_2, WSe_2, and MoS_2 (*17*, *18*). Because of the reduced Coulomb screening effects in lower dimensions, these monolayer TMD materials have much stronger exciton binding energies (in the range of 0.2 to 0.4 eV) so that excitons may be trapped and PL from radiative recombination of excitons can still be observed at room temperature (RT) (*19*). In addition, these atomically thin TMD materials (on the order of 0.6 nm) can be more easily fabricated by various deposition techniques than GaAs-based quantum wells. These attributes of TMDs are therefore promising for developing practical excitonic devices. However, the exciton strength in the PL spectra of TMD monolayers at RT is often substantially suppressed probably because of various defects (e.g., vacancies, impurities, surface degradation, etc.) that behave as nonradiative exciton recombination sites and reduce the quantum efficiency (*20*). In addition, defects in the monolayers may result in reduced binding energies for the electron-hole pairs and may contribute to excess doping that increases the Coulomb screening effects (*21*). These natural defects in the monolayer TMDs can give rise to the formation of impurity states near the Fermi level, leading to a large number of free carriers that can be easily coupled with excitons and form positive and negative trions (*22*). Hence, ideal TMD-based excitonic devices that are operational at RT are still not feasible so far (*23*). Various methods have been explored to reduce the defects and to enhance the excitonic behavior in monolayer TMDs, including chemical synthesis (*24*), gate voltage control (*25*), and magnetic field (*26*).

The orbital angular momentum (OAM) of light with helical wavefronts having a well-defined OAM $\ell\hbar$ per photon was first demonstrated in 1992 by Allen *et al.* (*27*). When light carrying a finite OAM illuminates on a sample, a net force is applied to the material as the result of nonuniform field distributions (*28*, *29*). In addition, an OAM is transferred to the material, leading to the manifestation of different degrees of freedom of light (*30*, *31*). In our previous studies, we investigated the effect of OAM light on the excitonic properties of monolayer MoS_2 and revealed an unusual light-like exciton band dispersion of valley excitons (*32*). We expect that further application of OAM to the studies of light-matter interaction can lead to more findings, because this process can provide notable control of the excitonic behaviors at RT without the need for any surface treatments of the sample or the application of external electric/magnetic fields.

In this work, we present a new approach to enhancing the excitonic behavior in monolayer tungsten disulfide (WS_2) by applying OAM of light, also known as twisted light (*28*). We find that the excitonic behavior and the contribution of trions in WS_2 monolayer

[1]Department of Physics, National Taiwan Normal University, Taipei, Taiwan. [2]Department of Physics, California Institute of Technology, Pasadena, CA 91125, USA.
*Corresponding author. Email: ncyeh@caltech.edu (N.-C.Y.); ywlan@ntnu.edu.tw (Y.-W.L.); thlu@ntnu.edu.tw (T.-H.L.)

can be controlled at RT using different topological charges and powers of OAM light and propose a phenomenological model to account for the interaction of OAM light with monolayer TMDs. Our findings further demonstrate that OAM of light can command the inter- and intravalley transitions in TMD materials, which offers a pathway to tuning optical devices.

RESULT AND DISCUSSION

Monolayer WS_2 flakes were grown on SiO_2 (300 nm)/Si substrate via the chemical vapor deposition (CVD) technique (*33*). Twisted light with different topological charges was generated by a spatial light modulator (SLM) and integrated with an in-house PL and Raman setup, as schematically shown in Fig. 1A. The OAM light was illuminated onto the monolayer WS_2 sample to study the excitonic behavior from the resulting PL spectra. The laser was a continuous wave, and the excitation wavelength was 532 nm.

The horizontally polarized light was collimated to a phase-only SLM of 1920 pixels by 1080 pixels with a pixel pitch of 8 μm. The phase patterns of different ℓ values were displayed on the SLM through a computer-generated hologram, which converted the incident beam into twisted light. The phase variations of twisted light with various odd numbers of ℓ are shown in Fig. 1B. The twisted beam passed through a beam reducer and was focused on the monolayer WS_2 flake by a 50× long working distance objective lens. The optical microscopy image of the WS_2 flake is shown in Fig. 1C. The fabricated WS_2 flakes are monolayer, which have been confirmed by atomic force microscopy (AFM) and Raman spectroscopy, as shown in fig. S1. Figure 1 (D and E) is the spatially resolved PL and Raman intensity maps of the monolayer WS_2 under the illumination of a Gaussian beam (ℓ = 0), and the maps show that the PL and Raman (E^1_{2g}) signals were uniform throughout the sample. The excitonic behavior in the PL spectra of WS_2 sample was studied and analyzed as a function of different OAM ℓ values and different laser powers on the sample surface.

The formation of excitons is often accompanied by trions, especially under the high laser power excitation. Figure 2A shows the PL spectra under different excitation laser powers from 100 to 800 μW. While the PL intensities associated with both neutral excitons and trions increase steadily with increasing power, contributions from trions apparently increased much faster with increasing power than excitons. This phenomenon may be attributed to heating and strain-induced formation of defect states under high laser power (*20*, *34*). Given that the increase in laser power has different effects on the formation of trions and excitons within the monolayer WS_2, an alternative approach to better controlling the quasiparticles must be devised. Figure 2B displays the PL spectra under different excitations of OAM light from ℓ = 0 to 5 at a fixed power of 800 μW. The decreasing PL intensity of WS_2 with the increasing value of the topological charge of light (ℓ) may be attributed to the decreasing power density on the sample due to the increasing OAM beam size with ℓ. Figure 2C depicts the deconvoluted PL spectrum with ℓ = 0 excitation to distinguish the exciton and trion peaks. The blue, red, and gray lines are fitting curves signifying the neutral excitons, trions, and defect states, respectively. Detailed analysis of the PL spectra taken at each constant power, as exemplified in Fig. 2B and fig. S2, reveals that the trion intensity steadily decreases with the increasing topological charge of the OAM light. This demonstration of controlling the formation of trions by OAM light presents a novel approach to achieving exciton-rich monolayer WS_2.

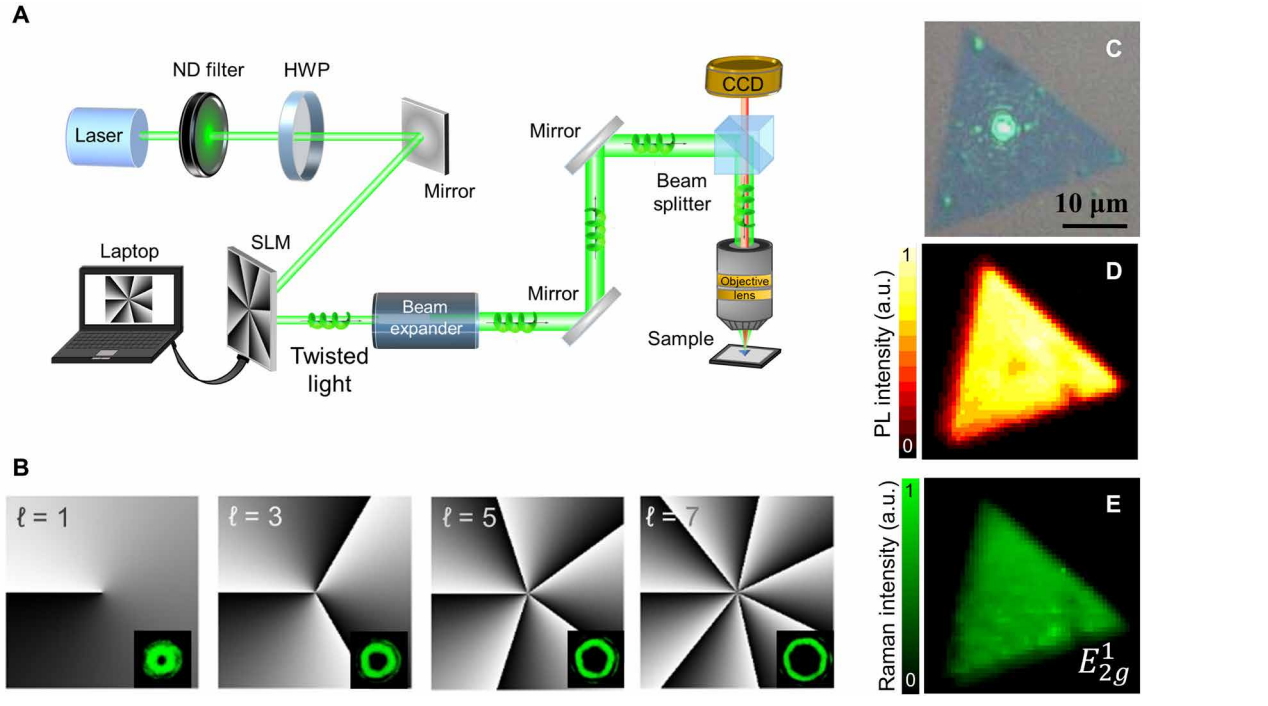

Fig. 1. Experimental setup and optical results of a CVD-grown monolayer WS_2. (**A**) Schematic of the PL and Raman spectroscopy setup for optical beam carrying OAM. CCD, charge-coupled device. ND filter, neutral density filter; HWP, half-wave plate. (**B**) Phase variations of the incident optical beam with different OAM values, ℓ. (**C**) Optical microscopy image of an as-grown monolayer WS_2 flake on SiO_2/Si substrate. (**D** and **E**) Intensity maps of the PL and Raman (E^1_{2g}) mode of the monolayer WS_2 sample shown in (C). a.u., arbitrary units.

To mitigate the heating-induced formation of defect state, we investigated the PL spectra taken at 77 and 300 K under a lower laser power (≤100 μW) for different values of OAM (ℓ = 0 to 8) and extracted the dependence of trion and exciton intensities on the OAM. Figure 3 (A and B) illustrates the deconvolution of PL spectra that distinguishes the exciton and trion peaks under the fundamental mode (ℓ = 0) and odd-numbered OAM light excitation at 300 and 77 K on a fixed laser power of 30 μW, respectively. We note that the full width at half maximum (FWHM) linewidths of all three peaks under the fundamental mode (ℓ = 0) became narrower from 300 to 77 K.

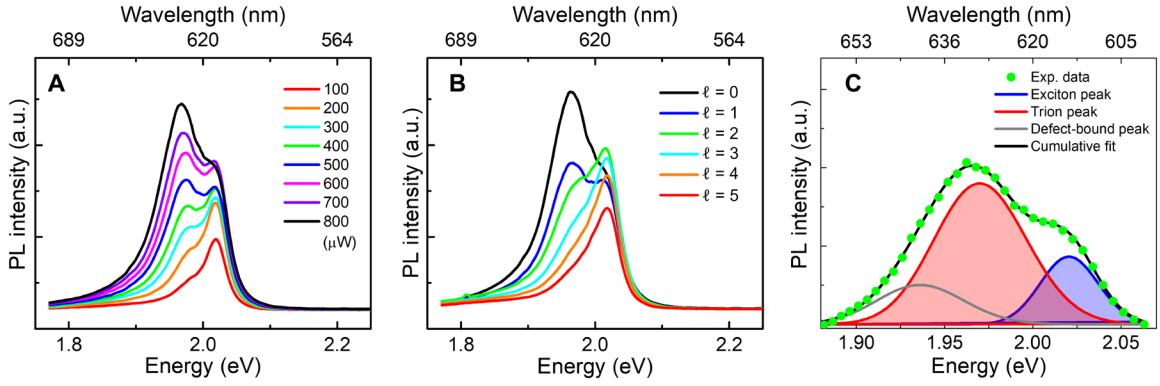

Fig. 2. Power and OAM light dependence PL of the monolayer WS_2. (**A**) PL spectra of monolayer WS_2 excited by the fundamental mode of light ℓ = 0 under different laser powers from 100 to 800 μW. (**B**) Control the trion intensity by different OAM lights (ℓ = 0 to 5) at a fixed laser power of 800 μW. (**C**) Theoretical fitting to the spectrum taken with ℓ = 0 and 800 μW of power, which reveals contributions from different components of the neutral excitons (blue), trions (red), and defect states (gray).

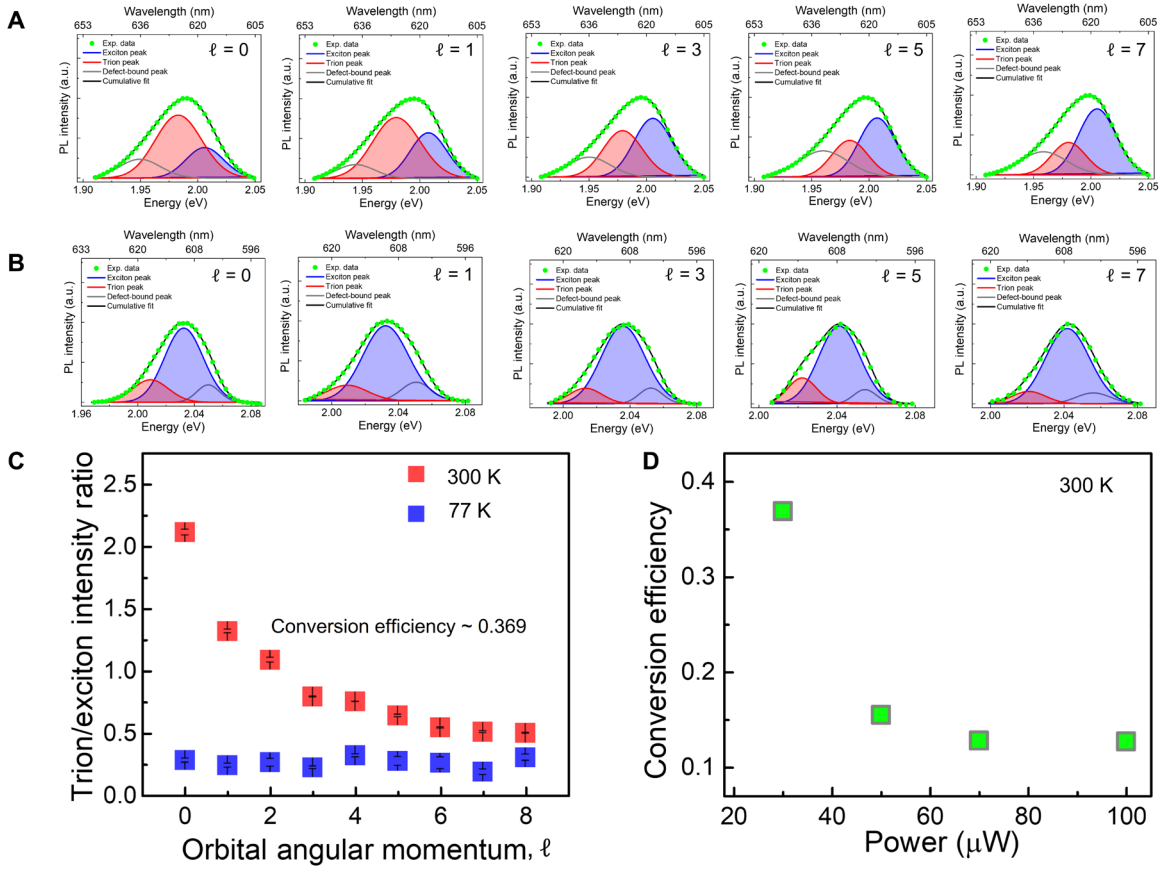

Fig. 3. OAM light dependence PL of the monolayer WS_2. Deconvoluted PL spectra of a monolayer WS_2 for an odd number of topological charges of OAM light with a laser power of 30 μW at (**A**) 300 K and (**B**) 77 K. The theoretical fitting to the spectrum represents the contributions from excitons (blue), trions (red), and defect states (gray). (**C**) Comparison of the variations of the trion/exciton intensity ratio with the OAM value ℓ under a constant laser power of 30 μW at 300 K (red squares) and 77 K (blue squares). (**D**) Trion-to-exciton conversion efficiency at 300 K as a function of the laser power.

For other OAM excitations, the deconvolution of PL spectra and detailed fitting for different contributions and parameters are shown in figs. S2 and S3 and tables S1 and S2, respectively. Although the deconvoluted third peak (gray color) in the PL spectra (Fig. 3, A and B) at ~640 nm (1.937 eV) and ~605 nm (2.049 eV) for RT and 77 K, respectively, was referred to as a defect peak in both cases, the nature of the corresponding defects at RT and 77 K was different: At RT, the defect peak at ~640 nm may be attributed to bound excitons (*35*), while the low-temperature defect peak at ~605 nm was found to be associated with the activation of shallow localized states (*36*). We have assessed the dependence of exciton and trion intensities on the OAM light and laser power by estimating the number of trions converted into excitons with increase ℓ from the trion-to-exciton intensity ratio. Figure 3C exhibits the trion-to-exciton intensity ratio extracted from Fig. 3 (A and B) with different OAM light excitations. This analysis implies the substantial transformation of trions into excitons with increasing topological charge up to ℓ = 5, beyond which the trion-to-exciton intensity ratio ($I_{trion}/I_{exciton}$) saturates. For comparison of the cases with different laser powers, we also performed similar experiments for the trion/exciton intensity ratio at 300 K and found that the trion/exciton intensity ratio increases with increasing laser power for each fixed value of OAM, as shown in fig. S4. After exponentially fitting the trion-to-exciton intensity ratio versus topological charge ℓ for a given power using the relation ($I_{trion}/I_{exciton}$) = c_0 exp. ($-\gamma/\ell$), with c_0 being a numerical constant, the coefficient γ that represents the efficiency of trion-to-exciton conversion with increasing OAM under a constant power can be estimated. We define the conversion efficiency γ as a coefficient that represents the ratio of the decreasing trion population to the corresponding increasing exciton population as a function of ℓ at a constant laser power. Figure 3C depicts the ($I_{trion}/I_{exciton}$) versus ℓ dependence under a constant power of 30 μW at 300 and 77 K, while the comparison of the γ values at 300 K under different laser powers is provided in Fig. 3D. It shows that the conversion efficiency is very high at low laser power and decreases exponentially with increasing power, which implies that the OAM light can suppress trions efficiently at low power. Detailed analyses of the PL spectra of monolayer WS_2 for the other laser powers (50, 70, and 100 μW) at 77 and 300 K are given in figs. S5 to S8. Furthermore, we have also conducted a control experiment that combines twisted light with electrostatic gating and found that OAM light can effectively reduce the free electron concentration and suppresses trion formation. The effect of gate voltage on the trion-to-exciton conversion efficiency of the WS_2 sample for 100-μW laser power at 300 K is shown in figs. S9 and S10. We further note that we did not perform further PL measurements at lower temperatures (<77 K) because the trion-to-exciton intensity ratio taken at 77 K with a fixed laser power was already nearly independent of the OAM value (ℓ) of light as shown in Fig. 3C.

To gain further insights into the effect of OAM and laser power on trions and excitons, we examined the FWHM linewidths of the PL spectra, because the behavior of excitons and trions in the material, including intra- and intervalley trions, may be dependent on their interactions with different OAM values of light (*37*). Figure 4 (A and B) shows the three-dimensional (3D) plot of the trion and exciton FWHM at 300 K as a function of the topological charge of OAM light and the laser power, respectively. As evidenced in Fig. 4A, the trion FWHM linewidth decreases rapidly with increasing OAM and increases slightly with laser power. The dependence on the OAM may be understood in terms of the presence of both intra- and intervalley trions: When monolayer WS_2 interacts with fundamental light (ℓ = 0), both intravalley (dominant) and intervalley (secondary) trions can be excited, which result in a relatively large FWHM linewidth (*38*). On the other hand, when monolayer WS_2 is excited by twisted light with ℓ ≠ 0, the probability of forming intravalley trions is suppressed with increasing ℓ, as manifested by the decreasing FWHM linewidth. In contrast, the exciton FWHM linewidth does not exhibit substantial variations with either the OAM or laser power, as shown in Fig. 4B. In particular, we note that the OAM light evidently affects the trion properties without disturbing the exciton characteristics in the monolayer WS_2. Detailed FWHM linewidth analyses of the exciton and trion states extracted from the PL spectra at 77 K are given in fig. S11, where the exciton FWHM is found to be nearly independent of either the OAM or the laser power and the trion FWHM exhibits a slight decrease with increasing OAM for the laser power at 30 and 50 μW.

The enhancement of the density of exciton quasiparticles due to the suppression of trions is highly dependent on the binding energy of the trion and the concentration of unbound electrons at the Fermi level (*39*, *40*). A higher value of trion binding energy corresponds to a stronger Coulomb interaction between the exciton and an unbound electron (*41*). The splitting between the exciton and trion energies is predicted to be linearly dependent on the Fermi energy (E_F) and is defined as (*42*)

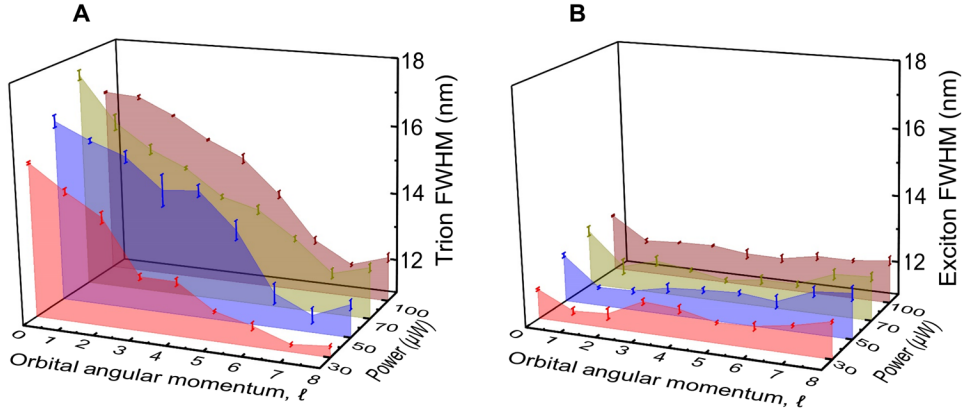

Fig. 4. FWHM analysis of trion and exciton from deconvoluted PL spectra. FWHM linewidths of the PL spectral intensities taken at 300 K are shown as a function of the OAM of light and laser power after deconvolution for contributions from (**A**) trions and (**B**) excitons, respectively.

$$E_{Xo} - E_{X-} = E^b_{X-} + E_F \quad (1)$$

where E^b_{X-} is the trion binding energy, E_{Xo} and E_{X-} are the energy levels of excitons and trions, respectively. Because an exciton can be considered as an ionized trion, ($E_{Xo} - E_{X-}$) defines the minimum energy required to remove one electron from the trion. Hence, the density of trions is proportionally dependent on the unbound electron density at the defect/Fermi level. The native defect density in the material corresponds to the unbound electron concentration responsible for the formation of trions (*43*), and the defect concentration may be derived from the mass action law, which is a theory used to estimate the defect concentration in 2D materials optically (*22*). Therefore, the density of unbound electrons associated with defects at the Fermi level may be estimated accordingly (*44*).

Siviniant *et al.* (*45*) first proposed the mass action law for excitons and trions, which is given by the following expression

$$\frac{n_{Xo}\, n_{e-}}{n_{X-}} = K(T) = \frac{4\, m_{\text{eff}} K_B T}{\pi \hbar^2} \exp\left(-\frac{E^b_{X-}}{K_B T}\right) \quad (2)$$

where n_{Xo}, n_{X-}, and n_{e-} are the concentrations of excitons, trions, and unbound electrons at the Fermi level of monolayer WS_2, respectively. m_{eff} is the reduced effective mass of monolayer WS_2, k_B is the Boltzmann's constant, T is the temperature, $\hbar$ is the reduced Plank's constant, and E^b_{X-} is the binding energy of the trions. The concentration of trion/exciton ratio is directly evaluated from the area of trion and exciton peak spectra in the PL spectra (*45*, *46*). The effective mass of monolayer WS_2 is defined by (*47*) $m_{\text{eff}} = \frac{m_{Xo} m^*_e}{m_{X-}}$, where $m^*_e = 0.31\, m_e$ is the effective electron mass, $m^*_h = 0.42\, m_e$ is the effective hole mass, $m_{Xo} = \frac{m^*_e m^*_h}{(m^*_e + m^*_h)}$ is the exciton mass, and $m_{X-} = \frac{m^*_e (m^*_e + m^*_h)}{(2\, m^*_e + m^*_h)}$ is the trion mass. The detailed calculation for the density of unbound electrons at the Fermi/defect level of WS_2 is provided in note S1.

Using Eqs. 1 and 2 and assuming that n_{Xo} and n_{X-} are proportional to the PL spectral weight of the exciton and trion peaks, respectively, we obtain estimated trion binding energies and unbound electron concentrations of monolayer WS_2 at 300 K in Fig. 5 (A and B), respectively, as functions of the OAM and laser power. In Fig. 5A, we find that the trion binding energy depends on the topological charge of the OAM light and the laser power. For low power (30 μW), the binding energy is around 24 meV for $\ell = 0$ and varies only slightly and nonmonotonically with increasing ℓ. When power increases from 50 to 100 μW, the trion binding energy increases from 31 to 36 meV for the fundamental mode of light ($\ell = 0$). A similar trend of increase in the trion binding energy E^b_{X-} with power is also found for $\ell > 0$. This increase in E^b_{X-} with power for a given ℓ may be attributed to the excess light–induced defect states in the material, which result in more unbound electrons at the defect level and therefore higher probabilities for the formation of trions. On the other hand, E^b_{X-} decreases with increasing ℓ from 1 to 8 for high powers of 50, 70, and 100 μW, as shown in Fig. 5A. In particular, a substantial decrease in E^b_{X-} is found from 36 meV with $\ell = 0$ to 27 meV with $\ell = 8$ under 100-μW laser power. This steady decrease in E^b_{X-} with increasing ℓ is consistent with the rapid decrease in $I_{\text{trion}}/I_{\text{exciton}}$ with ℓ in Fig. 3C. In addition, the substantial decrease in E^b_{X-} by 9 meV from $\ell = 0$ to $\ell = 8$ for 100 μW further confirmed the reduction of intravalley trions (of a larger binding energy) and the enhancement of intervalley trions (of a smaller binding energy) with increasing ℓ (*48*). Similarly, we find in Fig. 5B that the concentration of unbound electrons at the defect level decreases with increasing OAM of light. The estimated unbound electron densities associated with intrinsic defects via the mass action law agree well with previous reports that estimated the defect concentration through different means (*49*, *50*).

When light having OAM illuminates on a sample, there is a net force applying to the material and a torque acting on the electron and atom according to the relation $\frac{\langle \dot{L}_z \rangle}{P} = \frac{\ell}{\omega_B}$, where P is the total power in the beam, $\langle \dot{L}_z \rangle = \Gamma$ is the torque exerted upon an object, and ω_B is the angular frequency of the beam (*51*). It implies that the torque acting on the object is directly proportional to the topological charge of light at fixed power. The OAM light exerting a torque on the atom and molecules can control the induced current in devices (*28*–*31*), which implies that the OAM light can affect and trap unbound electrons at a defect level in the WS_2 sample by applying a torque. The concentration of unbound electrons at the defect level decreases with increasing OAM of light as shown in Fig. 5B, which may be attributed to OAM light–induced nonzero torque on electrons at the defect level/conduction band (*51*), leading to the reduction of unbound electrons and the suppression of intravalley trions with increasing ℓ. While the unbound electron concentration decreases rapidly with the OAM for $\ell \leq 5$, it becomes almost a constant for higher values of OAM ($\ell > 5$) even after increasing the laser power. In addition, the concentration of unbound electrons for $\ell > 0$ increases slightly with increasing power of up to 50 μW and then saturates at higher powers. We further note that we have also

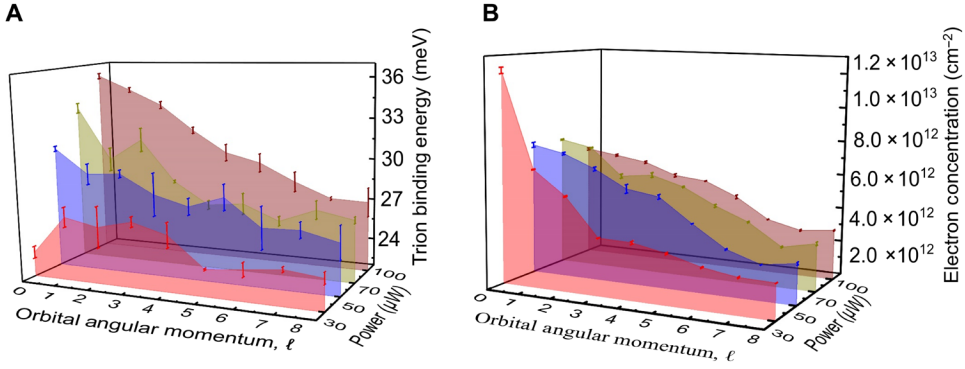

Fig. 5. Data analysis of the trion binding energy and the unbound electron concentration. (**A**) Estimation of the binding energy (E^b_{X-}) of trions with different OAM values and laser powers at 300 K. (**B**) Dependence of the unbound electron concentration (n_{e-}) on the OAM and laser power at 300 K.

investigated the PL spectra of several monolayer WS_2 and MoS_2 samples with different initial trion-to-exciton intensity ratios and found that the characteristics of the trion and exciton dependence on the OAM of light are all similar, which confirms the reliability of this method.

Proposed model for the mechanism of twisted light-matter interaction

The band structure of pristine monolayer WS_2 at the band edges K and K′ reveals a valence band splitting around 395 meV and a conduction band splitting around 17 meV as the result of spin-orbit coupling (*40*, *52*). In the presence of excess defect-induced electron doping, which is common among WS_2, the density of unbound electrons depends on the density of defects in the material, and the excess electrons associated with the defect level can be easily transferred to the conduction band. Previous studies have shown that, at high temperatures, unbound electrons are more likely to transfer from the defect level to the conduction band and form trions through Coulomb interactions with excitons (*53*). These trions may be divided into intravalley trions and intervalley trions, depending on whether the electrons coupled with the excitons are from the same or different valleys (*40*, *54*). Further studies of trions in the TMD material have indicated that intravalley trions have shorter lifetimes and larger FWHM than intervalley trion (*38*).

From our experimental results at RT, we have found that OAM light on monolayer WS_2 can effectively suppress the formation of trions and reduce both the FWHM of the PL peak and the binding energy of trions. To describe the OAM light–matter interaction with the electron-rich monolayer WS_2 film based on these experimental results (*40*), we propose a phenomenological model as depicted by the band structure diagrams in Fig. 6. Figure 6A shows that, under the excitation of fundamental light ($\ell = 0$), intravalley trions dominate over intervalley trions, which is consistent with our experimental findings of larger FWHM and binding energy of trions in Fig. 4A and Fig. 5A for $\ell = 0$. In contrast, as schematically illustrated in Fig. 6B, under OAM light illumination ($\ell \neq 0$), free electrons are affected by the OAM light–induced torque and become bound electrons, which reduces the probability of trion formation. In addition, intervalley trions become dominant over intravalley trions due to multipole interactions induced by OAM light, which is consistent with the experimental findings of smaller FWHM and binding energy of trions in Fig. 4A and Fig. 5A for $\ell \neq 0$.

When light carrying a finite OAM ($\ell \neq 0$) interacts with a suspended atom in the medium, a torque induced by the twisted light is exerted onto the atom (*51*). The strength of the torque depends on the value of the topological charge of the OAM and the power of light. In the case of monolayer WS_2, the illumination of OAM light may induce two effects. First, a finite torque induced by the twisted light provides an effective binding force acting on the unbound electrons in the conduction band, which affects the properties of charged trions without disturbing the neutral excitons (*51*). Second, larger topological charges can stimulate multipole transitions, thereby enhancing the intervalley transitions (*55*). Our observation of a substantial decrease in the trion binding energy from 36 meV for $\ell = 0$ to 27 meV for $\ell = 8$ under 100-μW laser power is strongly suggestive of the intervalley trion formation at larger OAM (*48*). In addition, the suppression of intravalley trions and the enhancement of neutral excitons with increasing ℓ as shown in Fig. 3C further corroborates the effects of OAM light. This interchangeable effect is also a well-known fingerprint of a trion-exciton pair in a PL spectrum (*56*). On

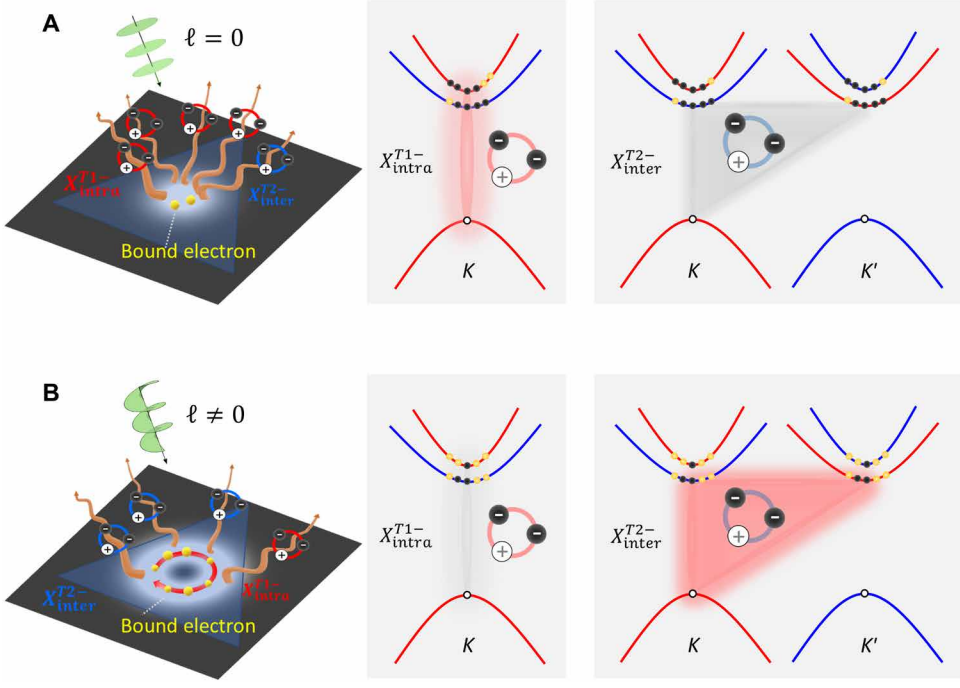

Fig. 6. Phenomenological model for OAM light–matter interaction. Schematic comparison of the interaction mechanism of monolayer WS_2 with excitation of (**A**) the fundamental mode of light ($\ell = 0$) where intravalley excitons/trions dominate over intervalley excitons/trions and (**B**) the twisted light ($\ell \neq 0$) where intravalley excitons/trions are suppressed and intervalley excitons/trions become dominant. Here, the red (blue) energy bands represent the spin-up (spin-down) bands, and X^{T1-}_{intra} and X^{T2-}_{inter} denote the intra- and intervalley trions, respectively.

the other hand, at sufficiently low temperatures, the unbound electrons are mostly frozen so that the torque from OAM light no longer helps reduce the unbound electron concentration or the trion density, which is consistent with our finding of negligible effects of OAM light on the trion-to-exciton ratio. Thus, our proposed phenomenological model provides a reasonable account for the effect of OAM light on controlling the trion behavior in monolayer TMDs.

In summary, we have investigated the effect of different topological charges of OAM light on the binding energies and FWHM of excitons and trions in monolayer WS_2 at 77 and 300 K. By systematically increasing the topological charge of OAM light from 0 to 8 for each value of the illuminating power from 30 to 800 μW, we analyze the evolution of the trion and exciton contributions to the PL spectra. It is found that, for low laser power and at 300 K, the trion-to-exciton intensity ratio decreases rapidly with increasing OAM up to $\ell = 5$ and then saturates for $\ell \geq 5$, while no discernible trion-to-exciton conversion is observable at low temperature (77 K). A feasible mechanism for the suppression of trions with increasing OAM is the exertion of nonzero torque, the unbound electrons in the monolayer WS_2 through the OAM light–matter interaction: The finite torque of OAM light interacts with WS_2 and results in a reduced concentration of unbound electrons at the defect level/conduction band, thereby reducing the probability of trion formation. In addition, OAM light is found to suppress intravalley trions and enhance intervalley trions. In contrast, OAM light has little effect on neutral excitons. Therefore, a notable enhancement of exciton emission can be achieved by applying OAM light to suppress the overall trion formation, which offers a new strategy to manipulate the PL spectra in monolayer TMDs for RT photonic and optoelectronic applications.

MATERIALS AND METHODS

Sample preparation

SiO_2/Si substrates (300-nm SiO_2) were used for the CVD growth of WS_2. Before the growth, SiO_2/Si substrates were cleaned in acetone and isopropyl alcohol for 30 min to remove organic impurities, then soaked in Nanostrip for 60 min, and lastly washed with deionized water and dried with nitrogen gas. For synthesis of monolayer WS_2, we used WO_3 and S as precursors in an atmospheric pressure CVD system to grow monolayer WS_2 on Si/SiO_2 substrates. Our setup includes the following parts: a quartz tube with a diameter of 2.54 cm and a length of 100 cm, a 2.54 cm–inner diameter horizontal split tube furnace (Lindberg/Blue M), and two mass flow controllers calibrated for Ar and H_2, with stainless steel flanges at both ends connected to a chiller water circulation system operating at 10°C. In the first step of the procedure, 95 mg of WO_3 precursor mixed with 5 mg of potassium iodide was placed in a quartz boat containing the SiO_2/Si substrates set face-down directly above the W source precursor, and the quartz boat was then positioned at the center of the furnace. A second boat containing 100 mg of S (Alfa Aesar; 99.999+%) was placed upstream at 16 cm away from the W source. Next, the system was pumped down to 3×10^{-2} torr to eliminate air and moisture. After the system reached the base pressure, the Ar/H_2 (80/40 standard cubic centimeter per minute) carrier gas was introduced until atmospheric pressure was achieved. The furnace was then heated up with a ramp rate of 35°C/min to the growth temperatures (750° to 850°C). The sulfur component melted at 150°C was sent into the furnace at the growth temperature to grow WS_2. The sample growth procedure proceeded for 10 min, after which the furnace was directly opened to RT to stop the reaction immediately (*33*).

Raman and PL spectroscopy

The Raman and PL spectra were acquired using a Kymera 328i spectrometer, and a backscattering configuration was performed using a 1200- and 150-line/mm grating, respectively. We used a continuous wave laser (model: LASOS DPSSL series, GLK 3320 TS01) of 532 nm as an excitation source. An Olympus 50× objective lens with a 0.50 numerical aperture was used for collecting light. Laser power was measured with a Thorlabs optical power meter. For OAM light generation, the SLM is a PLUTO phase only SLM by HOLOEYE. The SLM uses a panel (model: HED 6010 VIS) that operates optimally within the 420- to 700-nm wavelength range. It has a resolution of 1920 by 1080, with a reflectivity of around 65%, pixel pitch of 8 μm, and fill factor of 87%. The active area is 1.78 cm diagonal at the reflective optical mode. The cryogenic chamber made by Cryo Industries of America Inc. was used for low-temperature PL measurement (77 K).

Atomic force microscopy

The AFM measurements were performed in a noncontact tapping mode, using silicon tips with a Nanoview 1000 AFM (Utek Material).

SUPPLEMENTARY MATERIALS

Supplementary material for this article is available at https://science.org/doi/10.1126/sciadv.abm0100

REFERENCES AND NOTES

1. P. Tonndorf, R. Schmidt, R. Schneider, J. Kern, M. Buscema, G. A. Steele, A. Castellanos-Gomez, H. S. van der Zant, S. M. de Vasconcellos, R. Bratschitsch, Single-photon emission from localized excitons in an atomically thin semiconductor. *Optica* **2**, 347–352 (2015).
2. T. Mueller, E. Malic, Exciton physics and device application of two-dimensional transition metal dichalcogenide semiconductors. *npj 2D Mater. Appl.* **2**, 29 (2018).
3. L. Zhang, R. Gogna, W. Burg, E. Tutuc, H. Deng, Photonic-crystal exciton-polaritons in monolayer semiconductors. *Nat. Commun.* **9**, 713 (2018).
4. O. Lopez-Sanchez, D. Lembke, M. Kayci, A. Radenovic, A. Kis, Ultrasensitive photodetectors based on monolayer MoS_2. *Nat. Nanotechnol.* **8**, 497–501 (2013).
5. S. Wang, J. Wang, W. Zhao, F. Giustiniano, L. Chu, I. Verzhbitskiy, J. Zhou Yong, G. Eda, Efficient carrier-to-exciton conversion in field emission tunnel diodes based on MIS-type van der Waals heterostack. *Nano Lett.* **17**, 5156–5162 (2017).
6. Y. Ye, Z. J. Wong, X. Lu, X. Ni, H. Zhu, X. Chen, Y. Wang, X. Zhang, Monolayer excitonic laser. *Nat. Photonics* **9**, 733–737 (2015).
7. Y. Ye, J. Xiao, H. Wang, Z. Ye, H. Zhu, M. Zhao, Y. Wang, J. Zhao, X. Yin, X. Zhang, Electrical generation and control of the valley carriers in a monolayer transition metal dichalcogenide. *Nat. Nanotechnol.* **11**, 598–602 (2016).
8. D. Unuchek, A. Ciarrocchi, A. Avsar, K. Watanabe, T. Taniguchi, A. Kis, Room-temperature electrical control of exciton flux in a van der Waals heterostructure. *Nature* **560**, 340–344 (2018).
9. J. Xiao, Z. Ye, Y. Wang, H. Zhu, Y. Wang, X. Zhang, Nonlinear optical selection rule based on valley-exciton locking in monolayer WS_2. *Light Sci. Appl.* **4**, e366 (2015).
10. J. Xiao, M. Zhao, Y. Wang, X. Zhang, Excitons in atomically thin 2D semiconductors and their applications. *Nanophotonics* **6**, 1309–1328 (2017).
11. A. Raja, A. Chaves, J. Yu, G. Arefe, H. M. Hill, A. F. Rigosi, T. C. Berkelbach, P. Nagler, C. Schüller, T. Korn, C. Nuckolls, J. Hone, L. E. Brus, T. F. Heinz, D. R. Reichman, A. Chernikov, Coulomb engineering of the bandgap and excitons in two-dimensional materials. *Nat. Commun.* **8**, 15251 (2017).
12. H. Suchomel, S. Kreutzer, M. Jörg, S. Brodbeck, M. Pieczarka, S. Betzold, C. Dietrich, G. Sęk, C. Schneider, S. Höfling, Room temperature strong coupling in a semiconductor microcavity with embedded AlGaAs quantum wells designed for polariton lasing. *Opt. Express* **25**, 24816–24826 (2017).
13. S. Y. Bodnar, P. Grigoryev, D. Loginov, V. Davydov, Y. P. Efimov, S. Eliseev, V. Lovtcius, E. Ubyivovk, V. Y. Mikhailovskii, I. Ignatiev, Exciton mass increase in a GaAs/AlGaAs quantum well in a transverse magnetic field. *Phys. Rev. B* **95**, 195311 (2017).
14. S. Lourenço, I. Dias, J. Duarte, E. Laureto, V. Aquino, J. Harmand, Temperature-dependent photoluminescence spectra of GaAsSb/AlGaAs and GaAsSbN/GaAs single quantum wells under different excitation intensities. *Brazilian J. Phys.* **37**, 1212–1219 (2007).
15. J. Rojas-Ramírez, R. Goldhahn, P. Moser, J. Huerta-Ruelas, J. Hernandez-Rosas, M. López-López, Temperature dependence of the photoluminescence emission

from $In_xGa_{1-x}As$ quantum wells on GaAs(311) substrates. *J. Appl. Phys.* **104**, 124304 (2008).
16. G. Zhao, X. Liang, S. Ban, Binding energies of excitons in GaAs/AlAs quantum wells under pressure. *Modern Phys. Lett. B* **17**, 863–870 (2003).
17. C. Palacios-Berraquero, *Quantum Confined Excitons in 2-Dimensional Materials* (Springer, 2018).
18. L. Su, X. Fan, T. Yin, H. Wang, Y. Li, F. Liu, J. Li, H. Zhang, H. Xie, Inorganic 2D luminescent materials: Structure, luminescence modulation, and applications. *Adv. Optical Mater.* **8**, 1900978 (2020).
19. H. M. Hill, A. F. Rigosi, C. Roquelet, A. Chernikov, T. C. Berkelbach, D. R. Reichman, M. S. Hybertsen, L. E. Brus, T. F. Heinz, Observation of excitonic Rydberg states in monolayer MoS_2 and WS_2 by photoluminescence excitation spectroscopy. *Nano Lett.* **15**, 2992–2997 (2015).
20. S. Tongay, J. Suh, C. Ataca, W. Fan, A. Luce, J. S. Kang, J. Liu, C. Ko, R. Raghunathanan, J. Zhou, F. Ogletree, J. Li, J. C. Grossman, J. Wu, Defects activated photoluminescence in two-dimensional semiconductors: Interplay between bound, charged and free excitons. *Sci. Rep.* **3**, 2657 (2013).
21. K. Kaasbjerg, T. Low, A.-P. Jauho, Electron and hole transport in disordered monolayer MoS_2: Atomic vacancy induced short-range and Coulomb disorder scattering. *Phys. Rev. B* **100**, 115409 (2019).
22. K. Greben, S. Arora, M. G. Harats, K. I. Bolotin, Intrinsic and extrinsic defect-related excitons in TMDCs. *Nano Lett.* **20**, 2544–2550 (2020).
23. G. Grosso, J. Graves, A. Hammack, A. High, L. Butov, M. Hanson, A. Gossard, Excitonic switches operating at around 100 K. *Nat. Photonics* **3**, 577–580 (2009).
24. Y. Tao, X. Yu, J. Li, H. Liang, Y. Zhang, W. Huang, Q. J. Wang, Bright monolayer tungsten disulfide via exciton and trion chemical modulations. *Nanoscale* **10**, 6294–6299 (2018).
25. Z. Wang, H. Sun, Q. Zhang, J. Feng, J. Zhang, Y. Li, C.-Z. Ning, Excitonic complexes and optical gain in two-dimensional molybdenum ditelluride well below the Mott transition. *Light Sci. Appl.* **9**, 39 (2020).
26. H. Bragança, H. Zeng, A. C. Dias, J. H. Correa, F. Qu, Magnetic-gateable valley exciton emission. *npj Comput. Mater.* **6**, 90 (2020).
27. L. Allen, M. W. Beijersbergen, R. J. C. Spreeuw, J. P. Woerdman, Orbital angular momentum of light and the transformation of Laguerre-Gaussian laser modes. *Phys. Rev. A* **45**, 8185–8189 (1992).
28. M. Babiker, D. L. Andrews, V. E. Lembessis, Atoms in complex twisted light. *J. Optics* **21**, 013001 (2018).
29. P. K. Mondal, B. Deb, S. Majumder, Angular momentum transfer in interaction of Laguerre-Gaussian beams with atoms and molecules. *Phys. Rev. A* **89**, 063418 (2014).
30. Z. Ji, W. Liu, S. Krylyuk, X. Fan, Z. Zhang, A. Pan, L. Feng, A. Davydov, R. Agarwal, Photocurrent detection of the orbital angular momentum of light. *Science* **368**, 763–767 (2020).
31. J. Wätzel, J. Berakdar, Centrifugal photovoltaic and photogalvanic effects driven by structured light. *Sci. Rep.* **6**, 21475 (2016).
32. K. B. Simbulan, T.-D. Huang, G.-H. Peng, F. Li, O. J. Gomez Sanchez, J.-D. Lin, C.-I. Lu, C.-S. Yang, J. Qi, S.-J. Cheng, Selective photoexcitation of finite-momentum excitons in monolayer MoS_2 by twisted light. *ACS Nano* **15**, 3481–3489 (2021).
33. W.-H. Lin, W.-S. Tseng, C. M. Went, M. L. Teague, G. R. Rossman, H. A. Atwater, N.-C. Yeh, Nearly 90% circularly polarized emission in monolayer WS_2 single crystals by chemical vapor deposition. *ACS Nano* **14**, 1350–1359 (2020).
34. A. Bera, D. Muthu, A. Sood, Enhanced Raman and photoluminescence response in monolayer Mo_{S2} due to laser healing of defects. *J. Raman Spectroscopy* **49**, 100–105 (2018).
35. V. Carozo, Y. Wang, K. Fujisawa, B. R. Carvalho, A. McCreary, S. Feng, Z. Lin, C. Zhou, N. Perea-López, A. L. Elías, Optical identification of sulfur vacancies: Bound excitons at the edges of monolayer tungsten disulfide. *Sci. Adv.* **3**, e1602813 (2017).
36. J. Krustok, R. Kaupmees, R. Jaaniso, V. Kiisk, I. Sildos, B. Li, Y. Gong, Local strain-induced band gap fluctuations and exciton localization in aged WS_2 monolayers. *AIP Adv.* **7**, 065005 (2017).
37. M. Selig, G. Berghäuser, A. Raja, P. Nagler, C. Schüller, T. F. Heinz, T. Korn, A. Chernikov, E. Malic, A. Knorr, Excitonic linewidth and coherence lifetime in monolayer transition metal dichalcogenides. *Nat. Commun.* **7**, 13279 (2016).
38. T. P. Lyons, S. Dufferwiel, M. Brooks, F. Withers, T. Taniguchi, K. Watanabe, K. Novoselov, G. Burkard, A. I. Tartakovskii, The valley Zeeman effect in inter- and intra-valley trions in monolayer WSe_2. *Nat. Commun.* **10**, 2330 (2019).
39. J. J. Carmiggelt, M. Borst, T. van der Sar, Exciton-to-trion conversion as a control mechanism for valley polarization in room-temperature monolayer WS_2. *Sci. Rep.* **10**, 17389 (2020).
40. M. Drueppel, T. Deilmann, P. Krueger, M. Rohlfing, Diversity of trion states and substrate effects in the optical properties of an MoS_2 monolayer. *Nat. Commun.* **8**, 2117 (2017).
41. V. Huard, R. Cox, K. Saminadayar, A. Arnoult, S. Tatarenko, Bound states in optical absorption of semiconductor quantum wells containing a two-dimensional electron gas. *Phys. Rev. Lett.* **84**, 187–190 (2000).
42. K. F. Mak, K. He, C. Lee, G. H. Lee, J. Hone, T. F. Heinz, J. Shan, Tightly bound trions in monolayer MoS_2. *Nat. Mater.* **12**, 207–211 (2013).
43. X. Huang, Z. Li, X. Liu, J. Hou, J. Kim, S. R. Forrest, P. B. Deotare, Neutralizing defect states in MoS_2 monolayers. *ACS Appl. Mater. Interfaces* **13**, 44686–44692 (2021).
44. A. Vercik, Y. G. Gobato, M. Brasil, Thermal equilibrium governing the formation of negatively charged excitons in resonant tunneling diodes. *J. Appl. Phys.* **92**, 1888–1892 (2002).
45. J. Siviniant, D. Scalbert, A. Kavokin, D. Coquillat, J. Lascaray, Chemical equilibrium between excitons, electrons, and negatively charged excitons in semiconductor quantum wells. *Phys. Rev. B* **59**, 1602–1604 (1999).
46. J. S. Ross, S. Wu, H. Yu, N. J. Ghimire, A. M. Jones, G. Aivazian, J. Yan, D. G. Mandrus, D. Xiao, W. Yao, X. Xu, Electrical control of neutral and charged excitons in a monolayer semiconductor. *Nat. Commun.* **4**, 1474 (2013).
47. S.-Y. Shiau, M. Combescot, Y.-C. Chang, Trion ground state, excited states, and absorption spectrum using electron-exciton basis. *Phys. Rev. B* **86**, 115210 (2012).
48. G. Plechinger, P. Nagler, A. Arora, R. Schmidt, A. Chernikov, A. G. Del Águila, P. C. Christianen, R. Bratschitsch, C. Schüller, T. Korn, Trion fine structure and coupled spin–valley dynamics in monolayer tungsten disulfide. *Nat. Commun.* **7**, 12715 (2016).
49. P. Vancsó, G. Z. Magda, J. Pető, J.-Y. Noh, Y.-S. Kim, C. Hwang, L. P. Biró, L. Tapasztó, The intrinsic defect structure of exfoliated MoS_2 single layers revealed by scanning tunneling microscopy. *Sci. Rep.* **6**, 29726 (2016).
50. J. Hong, Z. Hu, M. Probert, K. Li, D. Lv, X. Yang, L. Gu, N. Mao, Q. Feng, L. Xie, J. Zhang, D. Wu, Z. Zhang, C. Jin, W. Ji, X. Zhang, J. Yuan, Z. Zhang, Exploring atomic defects in molybdenum disulphide monolayers. *Nat. Commun.* **6**, 6293 (2015).
51. C. E. Demore, Z. Yang, A. Volovick, S. Cochran, M. P. MacDonald, G. C. Spalding, Mechanical evidence of the orbital angular momentum to energy ratio of vortex beams. *Phys. Rev. Lett.* **108**, 194301 (2012).
52. A. Kuc, T. Heine, The electronic structure calculations of two-dimensional transition-metal dichalcogenides in the presence of external electric and magnetic fields. *Chem. Soc. Rev.* **44**, 2603–2614 (2015).
53. K. W. Böer, U. W. Pohl, in *Semiconductor Physics* (Springer International Publishing, 2019), pp. 1–35.
54. A. Arora, T. Deilmann, T. Reichenauer, J. Kern, S. M. de Vasconcellos, M. Rohlfing, R. Bratschitsch, Excited-state trions in monolayer WS_2. *Phys. Rev. Lett.* **123**, 167401 (2019).
55. A. Afanasev, C. E. Carlson, A. Mukherjee, High-multipole excitations of hydrogen-like atoms by twisted photons near a phase singularity. *J. Optics* **18**, 074013 (2016).
56. A. Esser, R. Zimmermann, E. Runge, Theory of trion spectra in semiconductor nanostructures. *Phys. Status Solidi B* **227**, 317–330 (2001).

Acknowledgments: We thank W.-H. Lin for developing the ML-WS_2 sample and useful discussions. **Funding:** This work was supported by the Ministry of Science and Technology, Taiwan under contract nos. MOST 109-2811-M-003-513, MOST 108-2112-M-003-010-MY3, and MOST 109-2112-M-003-002. N.-C.Y. acknowledges joint support by the National Science Foundation under the Physics Frontier Centers program for the Institute for Quantum Information and Matter (IQIM) at the California Institute of Technology (award #1733907) and the Army Research Office under the MURI program (award #W911NF-16-1-0472). **Author contributions:** The experiments were performed by R.K., K.B.S., T.-D.H., and Y.-F.C. The numerical calculation were completed by R.K., and Y.-F.C. provided assistance in performing the optical measurements. N.-C.Y., Y.-W.L., and T.-H.L. supervised this research. All authors have read and approved the manuscript. All authors discussed the results and commented on the manuscript. **Competing interests:** The authors declare that they have no competing interests. **Data and materials availability:** All data needed to evaluate the conclusions in the paper are present in the paper and/or the Supplementary Materials.

Submitted 20 August 2021
Accepted 10 February 2022
Published 1 April 2022
10.1126/sciadv.abm0100